AFRL-AFOSR-JP-TR-2019-0041

Rapid Preconcentration and Detection of Pathogens in Large Volumes via Dual-Nanoparticle targeting

Shalini Gupta
INDIAN INSTITUTE OF TECHNOLOGY DELHI
IIT CAMPUS HAUZ KHAS
NEW DELHI, 110016
IN

07/08/2019
Final Report

Air Force Research Laboratory
Air Force Office of Scientific Research
Asian Office of Aerospace Research and Development
Unit 45002, APO AP 96338-5002

REPORT DOCUMENTATION PAGE

Form Approved
OMB No. 0704-0188

1. REPORT DATE *(DD-MM-YYYY)*	2. REPORT TYPE	3. DATES COVERED *(From - To)*
08-07-2019	Final	28 Sep 2016 to 27 Mar 2019

4. TITLE AND SUBTITLE
Rapid Preconcentration and Detection of Pathogens in Large Volumes via Dual-Nanoparticle targeting

5a. CONTRACT NUMBER

5b. GRANT NUMBER
FA2386-16-1-4072

5c. PROGRAM ELEMENT NUMBER
61102F

6. AUTHOR(S)
Shalini Gupta

5d. PROJECT NUMBER

5e. TASK NUMBER

5f. WORK UNIT NUMBER

7. PERFORMING ORGANIZATION NAME(S) AND ADDRESS(ES)
INDIAN INSTITUTE OF TECHNOLOGY DELHI
IIT CAMPUS HAUZ KHAS
NEW DELHI, 110016 IN

8. PERFORMING ORGANIZATION REPORT NUMBER

9. SPONSORING/MONITORING AGENCY NAME(S) AND ADDRESS(ES)
AOARD
UNIT 45002
APO AP 96338-5002

10. SPONSOR/MONITOR'S ACRONYM(S)
AFRL/AFOSR IOA

11. SPONSOR/MONITOR'S REPORT NUMBER(S)
AFRL-AFOSR-JP-TR-2019-0041

12. DISTRIBUTION/AVAILABILITY STATEMENT
A DISTRIBUTION UNLIMITED: PB Public Release

13. SUPPLEMENTARY NOTES

14. ABSTRACT
The PI has had good success in this basic research project. In summary, the PI has demonstrated that the zwitterionic buffers are an ideal medium of choice for dielectric response measurements of colloidal suspensions irrespective of the particle type. HEPES in particular behaves like an anion at pH 8.5 but its unique molecular structure lends it a special status that cannot be explained by the current analytical models; the lower detection limit of 0.0025% w/v obtained in both Au NP and PS suspensions is unprecedented in the literature. Also, the long range particle-particle interactions become important at dilutions as low as 0.005 w/v % to 0.007 w/v %. There are 2 papers under preparation or under review as a direct result of this AOARD grant.

15. SUBJECT TERMS
bacterial tagging, magneto-electric fluid dynamics, pathogen detection

16. SECURITY CLASSIFICATION OF:			17. LIMITATION OF ABSTRACT	18. NUMBER OF PAGES	19a. NAME OF RESPONSIBLE PERSON
a. REPORT	b. ABSTRACT	c. THIS PAGE			CHEN, JERMONT
Unclassified	Unclassified	Unclassified	SAR		19b. TELEPHONE NUMBER *(Include area code)* 315-227-7007

Standard Form 298 (Rev. 8/98)
Prescribed by ANSI Std. Z39.18

Final Report for AOARD grant # FA2386-16-1-4072

Title: Rapid Pre-concentration and Detection of Pathogens in Large Volumes via Dual-Nanoparticle targeting

(Submission date: 10 June 2019)

List of publications and significant Collaborations that resulted from this AOARD project:

a) Papers published in peer-reviewed journals: None

b) Papers published in non-peer-reviewed journals or in conference proceedings: None

c) Conference presentations: Many in part (i.e., not fully dedicated to this work alone)

d) Manuscripts submitted but not yet published:
(i) Khandelwal A. V., Singh A., Pal N., Goel Goel G. and Gupta S. 'AC conductivity measurements of ultradilute colloidal suspensions using HEPES zwitterionic buffer', *Under review in Langmuir*

(ii) Anand S., Kaneriya N., Goel G. and Gupta S. 'Zwitterionic buffers: Ideal media for ultrasensitive AC conductivity measurements of colloidal suspensions', *Under preparation*

e) List any interactions with industry or with Air Force Research Laboratory scientists or significant collaborations that resulted from this work: Collaboration with Dr. Gaurav Goel, Dept. of Chemical Engineering at IIT Delhi

Abstract. Impedance spectroscopy is a highly sensitive and label-free technique to probe cellular suspensions. Our initial results with low concentrations of bacteria (1000 cells/mL) in different buffer media showed intriguing behaviour wherein, the impedance response varied in sign from negative to positive depending on the buffer type. Also, the sensitivity obtained with the zwitterionic buffer HEPES was significantly more than the standard PBS buffer. Therefore, impedance spectroscopy was used to probe the AC conductivity of extremely dilute colloidal suspensions ($2.5 \times 10^{-5} \leq \Phi_{w/v} \leq 4.0 \times 10^{-2}$) comprising of polystyrene microspheres (PS; $\kappa a >> 1$ and $\zeta = -65$ mV) and gold nanoparticles (Au NPs; $\kappa a > 1$ and $\zeta = -26$ mV) in HEPES buffer. Particles were used as synthetic analogues of cells. When AC electric fields of strength 10 mV and 1 MHz were applied via 100 μm gap interdigitated microelectrodes across 10 μL samples, a highly resistive ($\theta_{capacitive} < 1^o$) and non-monotonic response was obtained with particle concentrations at steady state. While the suspensions were less resistive (than the buffer) below a critical concentration, they became more resistive above it. More interestingly, particle-particle interactions took place in suspensions with concentrations as low as 0.005 w/v %. We believe this unique behaviour is linked to the zwitterionic nature of the HEPES molecule that provides an ideal microenvironment for counterionic polarization around the particles. The exact mechanism of polarization in HEPES, however, still remains elusive as the current theoretical models for simple electrolytes fail to explain our data.

1. INTRODUCTION

Early detection of pathogens in peripheral bloodstream is crucial for successful treatment of diseases and prevention of antimicrobial drug resistance. In several cases such as enteric fever for example, the concentration of pathogens is typically too low to be directly detected by the currently popular techniques. **Fig. 1** shows the concentration values reported for the causative agent for typhoid, *S.typhi*, in clinical samples.[1] At such low concentrations, the presence of cells follows a Poisson distribution requiring analysis of larger volumes (5 to 10 mL) to eliminate false negative results. Another major hurdle is the segmentation of cells from within the samples. Rare cell isolation and enumeration has been an idea of interest in microfluidics for a while now.[2] Researchers have tried exploiting hydrodynamic, dielectrophoretic and magnetophoretic forces to selectively separate bacterial cells from biosamples. In this project, we proposed immunomagnetic capture of cells, a highly selective method for cell enrichment, followed by ultrasensitive impedance spectroscopy measurements for cellular quantification.[3] With a combination of both techniques, we aimed to achieve a low limit of detection (LOD) ($\leq$ 100 cells/mL) without the initial growth phase, which is the most time-consuming step in most diagnostic techniques in use today.[4]

Our initial approach. The first approach entailed using a single nanoparticle to achieve cell capture as the cells themselves contributed to the impedance signal response. This eliminated the need for dual nanoparticle targeting as initially proposed in this project. For this, the antibody-conjugated magnetic nanoparticles (Ab-MNPs) were prepared as described earlier.[5] 100 μL of this suspension was incubated with 7 mL of analyte containing *S.typhi* cells in 40 mM HEPES (pH 7.5) for 30 min. The final concentration of the cells and Ab-MNPs was kept constant at 10^3 cells/mL and ~ 10^{13} particles/mL, respectively, in all the experiments. Bovine serum albumin (BSA) was also added (0.015 w/v % final concentration) to reduce any non-specific interaction. The entire mixture was then loaded onto the PDMS chip and the chip was mounted on the iMC^2 device as shown in **Fig. 2** and described elsewhere.[5] Briefly, the PDMS chip consisted of a 7 mL sample loading chamber. It also contained a small 50 μL recovery chamber to which the cell-antibody-MNP conjugates were swept by the magnetic panel in iMC^2. Below this recovery chamber, a 100 μm interdigitated micro-electrode was kept to take rapid impedance measurements of the enriched, isolated sample. The narrow duct connecting the loading and recovery chamber was intentionally kept thin (1 mm dia) to prevent liquid passage due to negative capillary pressure. This allowed us to obtain a completely dry pellet of

MNP-Ab-cells without any memory of the original sample. This was done to avoid interference of the original sample matrix in our impedance results. The bottom of the chip was enclosed with Parafilm® pasted on a poly-acrylic sheet layer. The polyacrylic sheet provided the required strength and rigidity to the chip, and the Parafilm® enable seamless sweeping without non-specific adsorption of the target biomolecules and cells on the surface.

Impedance measurements were taken at a constant setting of 10 mV and 1 MHz frequency. The reason for choosing this high frequency was better signal to noise ratio (**Fig. 3a**). The complete description of how the impedance experiments were performed and why we achieved high signal to noise ratio at 1 MHz is provided later in this report. We started our experiments by testing different buffers including 150 mM PBS (pH 7.5) and 40 mM HEPES (pH 7.5 and 8.5) as possible candidates for resuspension of the dry pellet collected in the recovery unit at the end of the sweep cycle. Our results showed intriguing behaviour wherein, the impedance response varied in sign from negative to positive depending on the buffer type (**Fig. 3b**). *This led us to change the course of our project to first understand why the impedance response changes so drastically with the liquid medium and what is the role of HEPES buffer in giving such higher signal sensitivity compared to PBS*. To keep our experiments simple, we carried out this investigation using synthetic particles as analogues for bacterial cells.

Impedance theory of colloidal suspensions. Frequency spectrum of permittivity, i.e., the dielectric dispersion, of a colloidal suspension is a macroscopic manifestation of polarizability of the particles which is inclusive of the solid core of the charged particle along with its diffuse ionic atmosphere. Factors such as particle size, shape, zeta potential, and concentration and mobility of ions in the medium cooperatively affect the electrical state of the solid/liquid interface, and thereby, suspension permittivity. Theoretical models for electrokinetic response of a particle in the infinite dilution limit, i.e. where particle-particle interaction effects are not important, are well established.[6–10] These models show a quantitative comparison between theory and experiments after considering a finite mobility of ions in the dense part of the double layer and/or correcting for the effect of electrode polarization at low frequencies.[11–16]

Recent experimental work and theoretical development has focused on furthering the understanding of dielectric dispersion of concentrated suspensions which are of increased practical and technological importance.[17] The data on complex impedance of colloidal suspensions is typically reported in terms of dielectric and conductivity increments (with respect to medium). For the case of blocking electrodes, the complex conductivity of a

suspension ($K_s^*(\omega)$) is obtained from its experimentally measured impedance value ($Z_s(\omega)$) as (**eq. 1)**,[8]

$$\frac{1}{C_c\, Z_s(\omega)} = K_s^*(\omega) = i\omega\varepsilon_o\varepsilon_s^*(\omega) = i\omega\varepsilon_o\varepsilon_s'(\omega) + \omega\varepsilon_o\varepsilon''_s(\omega) \qquad (1)$$

where, C_c is the sample cell constant (m^{-1}), $\varepsilon_s'(\omega)$ and $-\varepsilon_s''(\omega)$ are the frequency-dependent real and imaginary parts of the complex relative permittivity of the suspension (ε_s^*), respectively, $\omega = 2\pi f$ is the angular frequency and ε_o is the permittivity of free space. The increments in the real and imaginary parts of the relative permittivity can be defined as (**eq. 2)**,

$$\begin{aligned} \Delta\varepsilon_s'(\omega) &= \varepsilon_s'(\omega) - \varepsilon_e' \\ \Delta\varepsilon_s''(\omega) &= \varepsilon_s''(\omega) - \varepsilon_e'' \end{aligned} \qquad (2)$$

where, ε_e' and $-\varepsilon_e''$ are real and imaginary parts of the medium's relative permittivity.

Lack of linearity in the dielectric response of suspensions, manifest by variation in the specific increments $\frac{\Delta\varepsilon_s''}{\varphi}$ and $\frac{\Delta\varepsilon_s'}{\varphi}$ with particle concentration Φ, at as small as 1% volume fraction prevent the use of dilute suspension models.[18] Cell-model theories of electrokinetics for concentrated suspensions[18,19] were applied to suspensions of PS spheres at volume fractions between 1% to 18%.[20,21] Experimental permittivity and conductivity spectra for 200 nm diameter particles suspended in 0.01 and 0.1 mM KCl showed significant differences from the infinite dilution theory for all volume fractions while the spectra for suspensions in 1 mM KCl agreed with the infinite dilution calculation.[21] The cell model predictions for the dielectric increment were shown to compare favorably with the experimental data only at low electrolyte concentrations with a consistent underestimation of the value of low-frequency plateau.[20,21] The cell model predicted a volume fraction-dependent dielectric increment at all electrolyte concentrations. The predictions for conductivity increment were quantitative at all frequencies and electrolyte concentrations. Later, the cell model was modified for the case of soft particles, that is, particles consisting of a rigid core and a polyelectrolyte membrane.[22] The presence of latter was shown to lead to a larger dynamic mobility and larger alpha (low frequency)-relaxation amplitude in comparison with hard particles with the same charge. Further, both the charge on the core and charge in the membrane were shown to be very important parameters for the electrokinetic response of soft particles.

Our new approach. We explored another system that showed significantly higher sensitivity in comparison with the standard system of hard charged particles and a simple electrolyte (e.g., PBS or KCl). Specifically, we investigated the effect of a zwitterionic electrolyte, HEPES, on the dielectric spectra of hard PS and Au particles. The dielectric spectra have previously been characterized for aqueous suspensions of liposomal vesicles of zwitterionic phospholipids.[23–25] Permittivity values higher than the one typical of a non-ionic bilayer were reported and the system was modeled by introducing an apparent surface charge density at both the inner and outer aqueous interface. We expect an even more interesting response for the case of colloidal suspensions in a zwitterionic electrolyte wherein the zwitterionic groups are not localized at the "solid" (lipid)-water interface as in the case of phospholipid vesicles. However, no theoretical models exist at present for predicting the dielectric response of such systems which are of interest from both fundamental point of view as well as for applications relating to the design of highly sensitive and miniaturized sensors.[3] Knowledge of dependence of electrokinetic behaviour of these systems on parameters such as particle characteristics, surface charge, and particle concentration will ultimately aid in application of dielectric spectroscopy in these areas. To this end, we used electrical impedance spectroscopy to systematically probe the conductivity of colloidal suspensions comprising of dielectric PS microspheres ($\kappa a >> 1$ and $\zeta = -65$ mV), metal Au NPs ($\kappa a > 1$ and $\zeta = -26$ mV) and metallodielectric Au-PS particle composites in HEPES buffer in the ultralow volume fraction range of $0.0025\% \leq \Phi_{w/v} \leq 4\%$.

2. MATERIALS AND METHODS

2.1 Materials. Carboxylate-modified 1 μm polystyrene (PS) beads with 0.16 C/m^2 surface charge density (IDC Invitrogen, USA); Acetone and tannic acid (Fisher-scientific); Sodium citrate, chloroauric acid ($HAuCl_4.3H_2O$), silver enhancement kit and 4-(2-hydroxyethyl)-1-piperazineethanesulfonic acid (HEPES) (Sigma-Aldrich); Silicone grease (Metroark); Polydimethylsiloxane (PDMS) and curing agent (Sylgard 184, USA); Phosphate buffered saline (PBS) tablets (Omnipure); Ultrapure deionized (DI) water (~ 18.2 Mohm.cm) (Millipore, India). All reagents were used as received unless otherwise stated.

2.2. Sample preparation. ***Buffer:*** 150 mM PBS buffer at pH 7.4 (containing 137 mM NaCl, 2.7 mM KCl and 10 mM phosphate buffer also known as 1X PBS) was prepared by dissolving one PBS tablet in 100 mL of DI water. Similarly, 40 mM HEPES buffer at pH 5.3 was prepared by reconstituting 3.8 g of HEPES powder in 400 mL DI water. The HEPES pH was further

adjusted to 8.5 by adding approx. 14 mL of 1 M NaOH. The buffer conductivities were measured using the Mettler Toledo Lab-731 ISM conductivity meter and the pH data were collected using the Eutech Instruments pH-7200 meter.

Latex: 1 mL of 4% w/v stock suspension of PS was washed twice via centrifugation at 10,375g for 10 min each to remove any surfactants, electrolytes or preservatives from the medium. The final pellet was resuspended in HEPES buffer and further diluted (with HEPES) to different concentrations down to 0.001% w/v.

Au NPs: Citrate-capped Au NPs of approx. 16 nm diameter were synthesized using the well-known Turkevich method.[26] Briefly, 5 mL of 1% w/v $HAuCl_4$ was mixed with 395 mL of DI water. Simultaneously, a reducing solution was prepared by mixing 20 mL of 1% w/v sodium citrate, 50 µL of 1% w/v tannic acid and 80 mL of DI water. The gold and the reducing solutions were then heated up to 60 °C separately and mixed together under constant stirring at 60 °C for 4 h. Once the solution turned wine red color indicating the formation of AuNPs, the suspension was quenched in an ice-bath and stored at 4 °C. The Au NPs were then centrifuged from 3000g to 12000g at intervals of 3000g for 15 min each and resuspended each time in HEPES. The final concentrations were adjusted as desired by further dilution in HEPES.

Metallodielectric particles: To prepare Au NP-coated PS particles, 20 µL of 2% w/v PS suspension was incubated with 1 mL of 1.12 nM Au NP suspension at room temperature for different time durations under continuous shaking at 50 rpm. Excess gold was removed by two successive washings at 10375g for 10 min each and the final Au-PS pellet were resuspended in HEPES. These Au-PS particles were further deposited with silver metal by preferential silver ion reduction on gold. For this, 20 µL of Au-PS suspension was incubated with 50 µL of silver enhancement solution for different time durations. Finally, the particles were washed thrice at 3100g for 15 min each and resuspended in HEPES.

2.3 Sample characterization. The particles were characterized using several optical and spectroscopic techniques. The morphology of the particles was determined by optical microscopy (Olympus BX53 mounted with Orca Flash 4.0 Hamamatsu CCD camera), transmission electron microscopy (TEM) (FEI Tecnai G2) and scanning electron microscopy (SEM) **(**Zeiss EVO 50). The concentration of the Au NPs was estimated using UV-visible absorbance spectroscopy (Shimadzu UV-2600).[27] The zeta-potentials of the particles were obtained via Malvern zetasizer MS-602.

2.4 Experimental setup and impedance measurements. The experimental setup consisted of a high precision LCR meter (Agilent E4980A, 20 Hz – 2 MHz) interfaced with planar interdigitated platinum microelectrodes (IDEs) on glass substrates (Micrux, Spain). Each microelectrode chip comprised of symmetrical finger electrodes of 80 μm width and 100 μm edge to edge spacing (**Fig. 4**). These microelectrodes were encapsulated in a 1.5 mm thick PDMS slab punched with a 4 mm diameter hole and sealed to the chip by heating at 75 °C for 5 min. 10 μL of sample was then inserted into the PDMS chamber after gentle homogenization by hand and the top was sealed by a glass coverslip via vacuum grease to avoid evaporation. An AC field of 10 mV was applied at a sweep of 1 kHz to 1 MHz frequency ($\Delta f = 1\ kHz$) and the data were collected every 2.5 min for 1 h. Each experiment was repeated at least thrice and the results were reported as the mean ± 1 SD. The electrodes were then reused after extensive washing with acetone and DI water.

3. RESULTS AND DISCUSSION

Our system comprised of an IDE connected to an LCR meter through which an AC field was applied across colloidal suspensions to measure their impedance response (Fig. 4). The first set of experiments was performed to identify a suitable medium for carrying out these measurements in order to obtain the highest sensitivity and lowest limit of detection of the particles. For this, time-dependent impedance spectra were recorded with three different media namely ultrapure DI water, PBS and HEPES by sweeping the frequency across 1 kHz to 1 MHz range. In all three cases, while the signals decreased rapidly with frequency especially in case of ultrapure DI water and PBS (**Fig. S1a**), there was no significant variation with time suggesting that the signals were stable (**Fig. S1b**). The absolute values of impedance were highest in water and lowest in PBS. This was expected as ultrapure DI water has significantly lower electrolyte concentration as compared to PBS. When the experiments were repeated with PS suspensions at two different particle fractions (0.01 and 4 w/v%), HEPES gave significantly higher signal to noise ratio than in PBS and DI water suggesting it was a more suitable medium for carrying out the colloidal measurements **(Table 1)**. Another important observation was that the increment in impedance changed sign with particle concentration in HEPES. This change in sign implied that the suspension transitioned from being more conductive to more resistive as $\Phi_{w/v}$ was increased.

3.1 Choice of working frequency. A lower bound on the operating frequency was determined on the basis of need to eliminate system artefacts due to electrode polarization in blocking electrodes. We performed this calculation for PBS since the standard equations for various characteristic frequencies associated with electrokinetic response of colloidal suspensions are not expected to be directly valid for zwitterionic buffers. The frequency below which charges can fully build-up a double layer close to the blocking electrodes (ω_p) was calculated as 9 kHz and the characteristic frequency beyond which the electrode polarization becomes negligible (ω_b) was estimated to be 2.4 MHz (see **SI** for calculations). As reported by Chassagne *et al.*, a correction term may be used for $\omega_p < \omega < \omega_b$ to correctly calculate the permittivity increment, $\Delta\varepsilon_s'$ (see eq. 2), whereas, no such correction is required for $\Delta\varepsilon_s''$.[28] **Fig. 5** shows the change in the correction term as a function of frequency. We see that the relative correction term drops below 10% at 1 MHz, circumventing the need for any correction due to electrode polarization. This frequency is also well below the Maxwell-Wagner-O'Konski relaxation frequency (ω_{MWO} ~ 0.4 GHz in our case) beyond which there is no more energy dissipation in the system. Based on these results, we report all our data at 1 MHz frequency in the subsequent sections.

3.2 Effect of particle concentration and type. Next, we wanted to probe the high signal to noise ratio and the change in signal sign observed with HEPES in Table 1. To do this, we performed a series of experiments with different particle volume fractions varying from as low as $\Phi_{w/v}$ ~ 0.001% to 4%. The frequency spectra of the suspensions at different concentrations showed the expected behaviour in terms of concentration-dependent alpha relaxation (i,e, ω_{rel} increased with Φ) (**Fig. S5**).[18] Further, the experiments were repeated with two other particle types, metal Au NPs and Au-PS metallodielectric composites, to determine the generality of the observed change in sign with particle concentration. The metallodielectric particles were prepared by passive physiosorbtion of Au NPs on latex surface (see **Figs. S2, S3** for details). Once again, the plots of ΔZ showed a non-monotonic signal response yielding negative values at low particle concentrations and positive ones at higher fractions in all the three cases (**Fig. 6**). The increase was also highly non-linear at "higher" concentrations (> 0.1 w/v %).

The observation that the concentration-dependent AC impedance of all colloidal suspensions, irrespective of the particle type, shows a similar trend appears counterintuitive in the first glance. Impedance, however, is a macroscopic manifestation of the polarizability of the particles - a constitutive response of both the particle core and its ionic atmosphere, and

largely depends on the system parameters. The theoretical work on the electrical conductivity of dispersions in fact has a long and distinguished history, beginning with Maxwell's calculation of the DC conductivity of a suspension of uncharged non-conducting spheres in a solvent of conductivity K_e. Maxwell's result, $K_s = K_e\left(1-\frac{3}{2}\phi\right)$, indicates that the suspension conductivity *decreases* with concentration, or in other words, the resistance *increases* with concentration.[29] The calculation of the DC conductivity of a charged particle in an ionic solvent is substantially more complicated due the variation in ion densities in the double layer and the polarization of the ionic cloud. Saville and collaborators and O'Brien derived results for this situation, accounting specifically for the conductivity of the solution outside the diffuse layer, the polarization of the ion densities, and the contribution to the conductivity from electromigration and electroosmosis within the double layer.[30 31] The sum of these effects yield a Maxwell-like expression, $K_s = K_e(1 + \Delta\sigma\phi)$, but now with a $\Delta\sigma$ that can take either sign, depending on the relative thickness of the double layer, κa and the zeta (ζ) potential. Here, '$1/\kappa$' is the Debye length and 'a' is the particle radius. Thus, the resistance of the suspension can decrease under appropriate conditions irrespective of the particle type. At higher concentrations, many-body effects will start to appear and may increase the suspension resistance.[18]

Maxwell-Wagner and leaky dielectric models for AC conductivity again yield the result that the complex conductivity can either increase or decrease at linear order in volume fraction. Indeed, the theoretical results of DeLacey and White show a clear increase in the AC conductivity for thick double layers and large ζ potentials.[7] We suspect that the initial decrease in resistance observed in our experiments is precisely of the type predicted by DeLacey and White at infinite dilution while the subsequent increase in resistance with increasing volume fraction may be attributed to many-body interactions.[18,32] What is intriguing though is that the many-body interactions in our system start to appear at an unprecedentedly low concentration of 0.005 w/v%, which is at least two orders of magnitude lower than that reported in the literature.[17] Since a majority of systems in the literature use water, simple electrolytes (e.g. KCl, NaCl) or simple buffers like PBS as a medium, we have good reason to believe that the high signal enhancement seen in our case is a result of the unique behaviour exhibited by HEPES which is a zwitterionic buffer.

In fact, when our experimental results were compared with O'Brien's analytical model, the model completely failed to capture the non-linear response of particles in HEPES whereas, a good agreement was observed with PBS (with a slight offset) (**Fig. 7** and **SI**). This is because

the model takes into account double layer polarization around a single particle and extrapolates the results for a system of particles using linear superposition. Thus, it is only valid in the concentration regimes where there are no particle-particle interactions. The model also treats the electrolyte ions as point charges and fails to account for their molecular structure, perturbation or rearrangement around the particle surface, which may become important in case of relatively long, zwitterionic molecules such as HEPES. We believe it is due to this reason that HEPES shows such extraordinary particle concentration resolution. It is important to note that O'Brien's analytical solution is valid only for large κa and high frequency ($\frac{\omega a^2}{D} \gg 1$) values, both of which are satisfied in our case as our PS particles are 1 μm in size (κa = 328) and our working frequency is 1 MHz ($\frac{\omega a^2}{D}$ = 1180).

A careful look at the real and imaginary parts of permittivity at 1 MHz as a function of particle volume fraction showed that our suspension behaved mainly as a lossy dielectric at all volume fractions (ε_s''>> ε_s' in **Figs. 8a & b**). See **SI** for detailed calculations of how real and imaginary parts of permittivity can be obtained from impedance measurements. Further, while the capacitive part, ε_s' remained constant throughout the concentration range, the conductive part, ε_s'' fell sharply accounting for the non-linear rise in conductivity at higher volume fractions (see Fig. 3). This confirmed that the sharp rise in impedance was indeed due to a rise in system resistance and not an artefact of electrode polarization or saturation effects (these would have changed ε_s' as well). To understand the dip in impedance seen at low particle volume fractions in Fig. 6, we also plotted the specific dielectric response as shown in **Figs. 8c** & **d**. Fig. 8d showed that the suspension was more conductive than the buffer at lower particle fractions and eventually became more resistive above a certain threshold. Most importantly, the slopes of the magnitudes of the capacitive (Fig. 8c) and conductive (Fig. 8d) components varied inversely with concentration. Hence, the combination of the two, namely the impedance, showed a minimum at some point (remember: $\Delta\varepsilon_s''$ >> $\Delta\varepsilon_s'$ at all concentrations) as seen in Fig. 6.

3.3 Role of surface conductivity in the AC response of colloidal suspensions. To confirm the role of counterionic layer on the impedance response of our system, we performed two experiments. In the first one, we coated the PS particles with a non-ionic surfactant Tween 20 in order to modulate their zeta-potential. The Tween 20 concentration was carefully chosen such that it was just enough to fully coat the particle surface (see **SI** for details). By doing this, the zeta potential of the particles dropped from approx. -65 to -23 mV (see **Fig. S6**). The

impedance experiments were then repeated for the most dilute PS suspension where it was more conductive than the buffer without surfactant. The results obtained clearly showed a change in sign as well as the change in slope of the net impedance value (akin to the AC conductivity response of a system with thin double layers and small ζ potentials) suggesting that the surface charges indeed play a role in the AC conductivity of colloidal suspensions (**Fig. 9a)**.

In the second experiment, we systematically suppressed the negative surface charge of the Au NPs by depositing silver metal (Ag^0) on top of them. For this, our metallodielectric composites were exposed to a silver salt solution in the presence of a suitable reducing agent in order to selectively grow silver nanoshells around the Au NPs (acting as nucleation sites) (see **Fig. S4**). The binding process itself was quite heterogeneous with the number of Au NPs varying significantly across different PS beads, however, the overall reduction in the negative charge (on the Au NPs) manifested into an increase in the suspension resistivity until a saturation was reached after ~ 3 min of silver enhancement (**Fig. 9b-d**). Both these approaches established the role of surface charge in the AC response of colloidal suspensions.

3.4 Role of HEPES buffer in the AC response of colloidal suspensions. Finally, we wanted to understand the role of HEPES in enhancing the sensitivity of impedance response in colloidal suspensions and the appearance of particle interaction (many-body) effects at a much smaller particle concentration than are observed for simple electrolytes, such as PBS in this work or KCl in Beltramo et al.[16] HEPES is a zwitterionic molecule that can exist in three charged states depending on the solution pH as shown in **Fig. 10a** (pKa_1 = 3, pKa_2 =7.5). At pH 8.5, where we performed all our experiments, the molecules are net negatively charged and as the pH is reduced to 5, the average charge per molecule tends to zero (**Fig. 10b** & **S7**). This is where a majority of the molecules exist in a weakly polarized zwitterionic state. A general understanding of our system led us to initially hypothesize that this charge duality on the HEPES molecule manifests into an expansion of the apparent Debye length around the particles due to layer-by-layer self-assembly of the HEPES molecules at the particle-solution interface. This is unlike the case of Tween 20 where the molecular adsorption is driven purely by hydrophobic interactions rather than electrostatic ones. To test the veracity of this hypothesis, we performed experiments in which the charge on the HEPES molecules was modulated by changing the pH of the buffer and the corresponding impedance response of the colloidal suspensions as well as the hydrodynamic diameter of the particles was measured. A strong absorption of HEPES molecules at the particle surface should manifest as increase in the

particle hydrodynamic diameter, with the magnitude of increase dependent on the number of adsorbed layers. The average Au NP size was found to change from 36 nm at pH 5 to 50 nm at pH 8.5 (**Fig. 11b**). These particle sizes are much smaller than the average particle-particle separation of 295 nm calculated at 0.01% particle fraction, the smallest concentration at which significant many-body effects are observed in Fig. 6.

Further, higher particle size at pH 8.5 where HEPES is a co-ion for the negatively charged particle (~ -1 charge on HEPES), in contrast with that at pH 5 (zero net charge, maximum charge separation in HEPES), indicates absence of any noticeable layer-by-layer assembly of HEPES on the Au NP surface. The net charge per HEPES molecule increases with increase in pH (as shown in Fig. 10b) and it leads to an increase in the impedance of colloidal suspension (Fig. 11a) reminiscent of the Fig. 6 experiments in which the decrease in zeta potential led to an increase in impedance. These results lead us to believe that primary effect of HEPES is similar to that of standard electrolytes where an increase in ionic concentration leads to an increased suppression of the counterionic double layer around the particles and hence, reduction in overall polarization. However, the reasons for secondary effect of much larger and longer-ranged particle-particle interactions in HEPES buffer compared to simple electrolytes are not understood and remain an open question in the field.

3.4 Generality of approach. When experiments were repeated with three other zwitterionic buffers having similar structure as HEPES, our results could be beautifully reproduced indicating that the underlying structure of the buffer molecules played an important role in the overall signaling process. More interestingly, the signal improved drastically in EPPS which has a single carbon atom greater than HEPES (**Fig. S8**). Studies are currently underway to investigate the effect of

CONCLUSIONS

In summary, we have demonstrated that the zwitterionic buffers are an ideal medium of choice for dielectric response measurements of colloidal suspensions irrespective of the particle type. HEPES in particular behaves like an anion at pH 8.5 but its unique molecular structure lends it a special status that cannot be explained by the current analytical models; the lower detection limit of 0.0025% w/v obtained in both Au NP and PS suspensions is unprecedented in the literature. Also, the long range particle-particle interactions become important at dilutions as low as 0.005 w/v % to 0.007 w/v %. Similar results were obtained with EPPS, POPSO and PIPES zwitterionic buffers. The overall particle polarizability is governed by the counterionic

double layer polarization around the particles and the suspensions are mainly resistive at all volume fractions. The impedance response is also highly non-linear at fractions > 0.1 w/v %. We hope these results will excite the application scientists to develop new sensors with ultrahigh sensitivity and at the same time lead to more fundamental research on zwitterionic buffers.

Acknowledgements. We would like to acknowledge Asian office of Aerospace Research and Development (AOARD) for funding (grant #16IOA072).

References

(1) Wain, J.; Diep, T. S.; Ho, V. A.; Walsh, A. M.; Hoa, N. T. T.; Parry, C. M.; White, N. J. Quantitation of Bacteria in Blood of Typhoid Fever Patients and Relationship between Counts and Clinical Features, Transmissibility, and Antibiotic Resistance. *Journal of Clinical Microbiology* **1998**, *36* (6), 1683–1687.

(2) Chen, Y.; Li, P.; Huang, P. H.; Xie, Y.; Mai, J. D.; Wang, L.; Nguyen, N. T.; Huang, T. J. Rare Cell Isolation and Analysis in Microfluidics. *Lab on a Chip*. 2014, pp 626–645. https://doi.org/10.1039/c3lc90136j.

(3) Pal, N.; Sharma, S.; Gupta, S. Sensitive and Rapid Detection of Pathogenic Bacteria in Small Volumes Using Impedance Spectroscopy Technique. *Biosensors and Bioelectronics* **2016**, *77*, 270–276. https://doi.org/10.1016/j.bios.2015.09.037.

(4) Hejazian, M.; Li, W.; Nguyen, N. T. Lab on a Chip for Continuous-Flow Magnetic Cell Separation. *Lab on a Chip*. 2015, pp 959–970. https://doi.org/10.1039/c4lc01422g.

(5) Singh, S.; Upadhyay, M.; Sharma, J.; Gupta, S.; Vivekanandan, P.; Elangovan, R. A Portable Immunomagnetic Cell Capture System to Accelerate Culture Diagnosis of Bacterial Infections. *Analyst* **2016**, *141* (11), 3358–3366. https://doi.org/10.1039/c6an00291a.

(6) Dukhin, S. S.; Shilov, V. N.; Bikerman, J. J. Dielectric Phenomena and Double Layer in Disperse Systems and Polyelectrolytes. *Journal of The Electrochemical Society* **1974**, *121* (4), 154C. https://doi.org/10.1149/1.2402374.

(7) DeLacey, E. H. B.; White, L. R. Dielectric Response and Conductivity of Dilute Suspensions of Colloidal Particles. *Journal of the Chemical Society, Faraday Transactions 2* **1981**, *77* (11), 2007. https://doi.org/10.1039/f29817702007.

(8) Mangelsdorf, C. S.; White, L. R. Dielectric Response of a Dilute Suspension of Spherical Colloidal Particles to an Oscillating Electric Field. *Journal of the Chemical Society, Faraday Transactions* **1997**, *93* (17), 3145–3154. https://doi.org/10.1039/a701289f.

(9) López-García, J. J.; Grosse, C.; Horno, J. On the Use of the Stern-Layer and the Charged-Layer Formalisms for the Interpretation of Dielectric and Electrokinetic Properties of Colloidal Suspensions. *Journal of Colloid and Interface Science* **2009**, *329* (2), 384–389. https://doi.org/10.1016/J.JCIS.2008.09.078.

(10) Fixman, M. A Macroion Electrokinetics Algorithm. *The Journal of Chemical Physics* **2006**, *124* (21), 214506. https://doi.org/10.1063/1.2198838.

(11) Kijlstra, J.; van Leeuwen, H. P.; Lyklema, J. Low-Frequency Dielectric Relaxation of Hematite and Silica Sols. *Langmuir* **1993**, *9* (7), 1625–1633.

https://doi.org/10.1021/la00031a005.
(12) Rosen, L. A.; Baygents, J. C.; Saville, D. A. The Interpretation of Dielectric Response Measurements on Colloidal Dispersions Using the Dynamic Stern Layer Model. *The Journal of Chemical Physics* **1993**, *98* (5), 4183–4194. https://doi.org/10.1063/1.465108.
(13) Arroyo, F.; Carrique, F.; Bellini, T.; Delgado, A. Dielectric Dispersion of Colloidal Suspensions in the Presence of Stern Layer Conductance: Particle Size Effects. *Journal of colloid and interface science* **1999**, *210* (1), 194–199. https://doi.org/10.1006/jcis.1998.5914.
(14) Arroyo, F. .; Carrique, F.; Delgado, A. . Effects of Temperature and Polydispersity on the Dielectric Relaxation of Dilute Ethylcellulose Suspensions. *Journal of Colloid and Interface Science* **1999**, *217* (2), 411–416. https://doi.org/10.1006/JCIS.1999.6396.
(15) Jiménez, M. L.; Arroyo, F. J.; van Turnhout, J.; Delgado, A. V. Analysis of the Dielectric Permittivity of Suspensions by Means of the Logarithmic Derivative of Its Real Part. *Journal of Colloid and Interface Science* **2002**, *249* (2), 327–335. https://doi.org/10.1006/JCIS.2001.8141.
(16) Beltramo, P. J.; Furst, E. M. Transition from Dilute to Concentrated Electrokinetic Behavior in the Dielectric Spectra of a Colloidal Suspension. *Langmuir* **2012**, *28* (29), 10703–10712. https://doi.org/10.1021/la301876w.
(17) Grosse, C.; Delgado, A. V. Dielectric Dispersion in Aqueous Colloidal Systems. *Current Opinion in Colloid & Interface Science* **2010**, *15* (3), 145–159. https://doi.org/10.1016/J.COCIS.2009.11.004.
(18) Carrique, F.; Arroyo, F. J.; Jiménez, M. L.; Delgado, A. V. Dielectric Response of Concentrated Colloidal Suspensions. *The Journal of Chemical Physics* **2003**, *118* (4), 1945. https://doi.org/10.1063/1.1531072.
(19) S. Ahualli, A. Delgado, S. J. Miklavcic, L. R. W. Dynamic Electrophoretic Mobility of Concentrated Dispersions of Spherical Colloidal Particles. On the Consistent Use of the Cell Model. **2006**. https://doi.org/10.1021/LA0607252.
(20) Bradshaw-Hajek, B. H.; Miklavcic, S. J.; White, L. R. Dynamic Dielectric Response of Concentrated Colloidal Dispersions: Comparison between Theory and Experiment †. *Langmuir* **2009**, *25* (4), 1961–1969. https://doi.org/10.1021/la8028963.
(21) Beltramo, P. J.; Roa, R.; Carrique, F.; Furst, E. M. Dielectric Spectroscopy of Concentrated Colloidal Suspensions. *Journal of Colloid and Interface Science* **2013**, *408*, 54–58. https://doi.org/10.1016/J.JCIS.2013.07.042.
(22) Ahualli, S.; Jiménez, M. L.; Carrique, F.; Delgado, A. V. AC Electrokinetics of Concentrated Suspensions of Soft Particles. *Langmuir* **2009**, *25* (4), 1986–1997. https://doi.org/10.1021/la803171f.
(23) Uhlendorf, V. Fatty Acid Contamination and Dielectric Relaxation in Phospholipid Vesicle Suspensions. *Biophysical Chemistry* **1984**, *20* (3), 261–273. https://doi.org/10.1016/0301-4622(84)87030-1.
(24) Pottel, R.; Göpel, K.-D.; Henze, R.; Kaatze, U.; Uhlendorf, V. The Dielectric Permittivity Spectrum of Aqueous Colloidal Phospholipid Solutions between 1 KHz and 60 GHz. *Biophysical Chemistry* **1984**, *19* (3), 233–244. https://doi.org/10.1016/0301-4622(84)87005-2.
(25) Di Biasio, A.; Cametti, C. Dielectric Properties of Aqueous Zwitterionic Liposome Suspensions. *Bioelectrochemistry* **2007**, *70* (2), 328–334. https://doi.org/10.1016/j.bioelechem.2006.04.004.
(26) Kimling, J.; Maier, M.; Okenve, B.; Kotaidis, V.; Ballot, H.; Plech, A. Turkevich Method for Gold Nanoparticle Synthesis Revisited. *Journal of Physical Chemistry B* **2006**, *110* (32), 15700–15707. https://doi.org/10.1021/jp061667w.

(27) Liu, X.; Atwater, M.; Wang, J.; Huo, Q. Extinction Coefficient of Gold Nanoparticles with Different Sizes and Different Capping Ligands. *Colloids and Surfaces B: Biointerfaces* **2007**, *58* (1), 3–7. https://doi.org/10.1016/j.colsurfb.2006.08.005.
(28) Chassagne, C.; Dubois, E.; Jiménez, M. L.; van der Ploeg, J. P. M.; van Turnhout, J. Compensating for Electrode Polarization in Dielectric Spectroscopy Studies of Colloidal Suspensions: Theoretical Assessment of Existing Methods. *Frontiers in Chemistry* **2016**, *4* (July), 1–19. https://doi.org/10.3389/fchem.2016.00030.
(29) Su, Y. H.; Tsegaye, M.; Varhue, W.; Liao, K. T.; Abebe, L. S.; Smith, J. A.; Guerrant, R. L.; Swami, N. S. Quantitative Dielectrophoretic Tracking for Characterization and Separation of Persistent Subpopulations of Cryptosporidium Parvum. *Analyst* **2013**, *139* (1), 66–73. https://doi.org/10.1039/c3an01810e.
(30) O'Brien, R. W. The Solution of the Electrokinetic Equations for Colloidal Particles with Thin Double Layers. *Journal of Colloid And Interface Science* **1983**, *92* (1), 204–216. https://doi.org/10.1016/0021-9797(83)90129-7.
(31) O'Brien, R. W. The High-Frequency Dielectric Dispersion of a Colloid. *Journal of Colloid And Interface Science* **1986**, *113* (1), 81–93. https://doi.org/10.1016/0021-9797(86)90208-0.
(32) Carrique, F.; Ruiz-Reina, E.; Arroyo, F. J.; Jiménez, M. L.; Delgado, Á. V. Dielectric Response of a Concentrated Colloidal Suspension in a Salt-Free Medium. *Langmuir* **2008**, *24*, 11544–11555. https://doi.org/10.1021/la802218j.
(33) Israelachvili, J. N. *Intermolecular and Surface Forces: Third Edition*; 2011. https://doi.org/10.1016/C2011-0-05119-0.

Figures

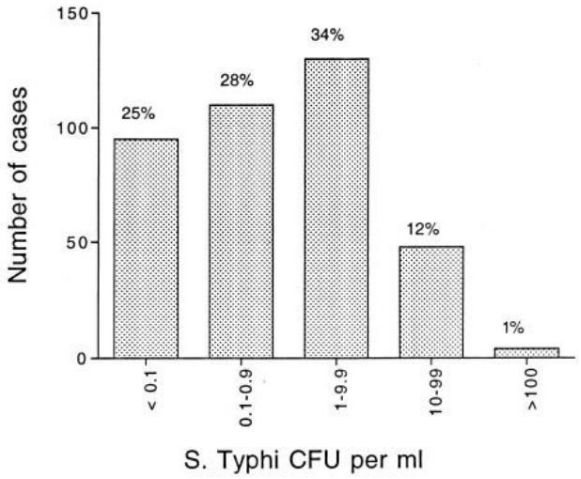

Figure 1. S.typhi concentration is typically < 10 CFU/mL in majority of typhoid cases, making direct detection difficult and error-prone (Graph taken from Ref. 1).

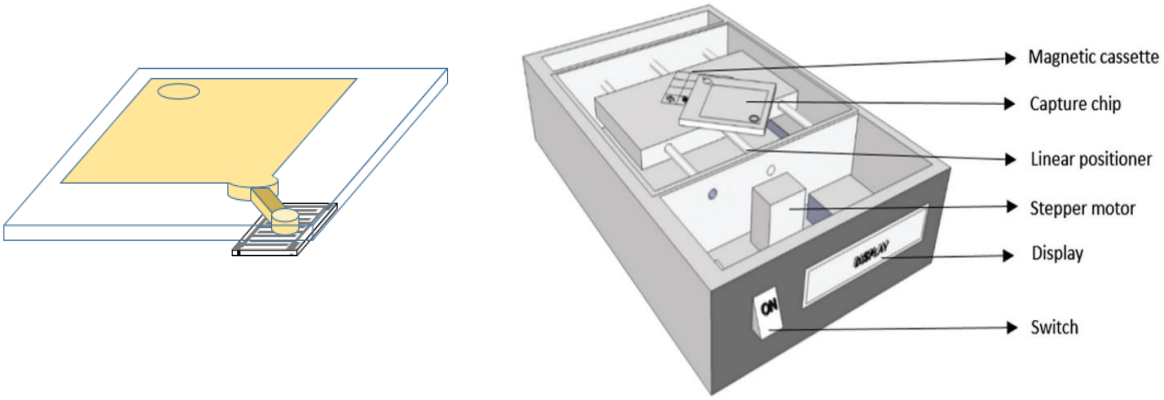

Figure 2. The PDMS capture chip isolates the recovery chamber from the loading chamber by a thin channel which prevents the flow of liquid into the recovery chamber. Schematic of the iMC^2 device. It consists of a diamond shaped neodymium magnet assembly upon which the chip is placed. A linear stepper motor is used to move the magnetic platform below the chip, sweeping and enriching the magnetized cell complexes into the miniature recovery unit (Schematics from Ref. 5).

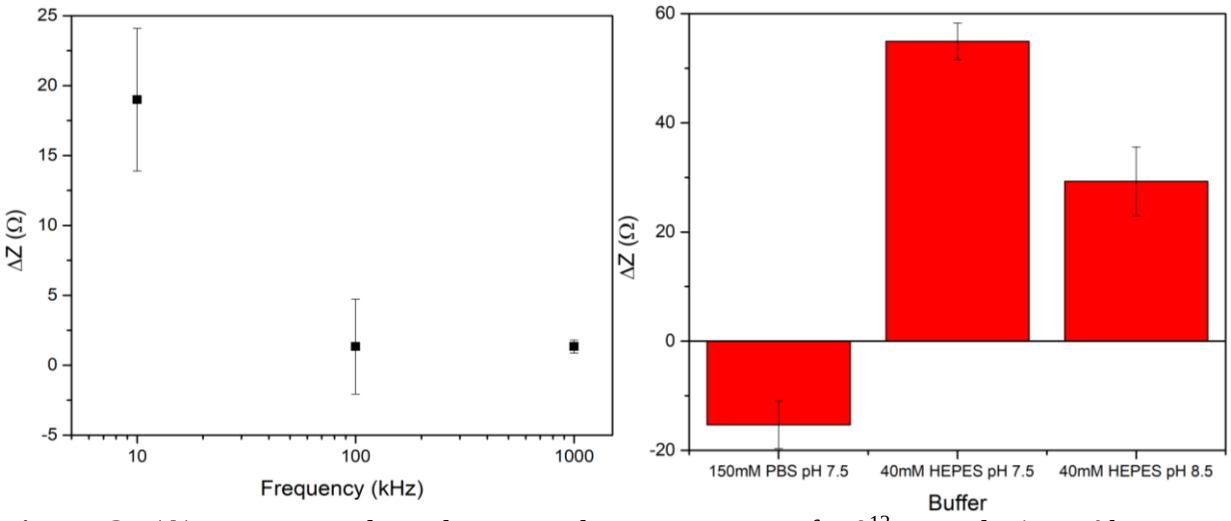

Figure 3. (A) Frequency-dependent impedance response of 10^{13} particles/mL Ab-MNP bioconjugates. The low signal to noise ratio at 1 MHz prompted us to use this frequency for all subsequent impedance measurements. **(B)** Effect of solvent on impedance response of 10^3 S.typhi cells/mL. 40 mM HEPES at pH 7.45 was selected for all further work. All Y-axis values are reported with respect to buffer alone.

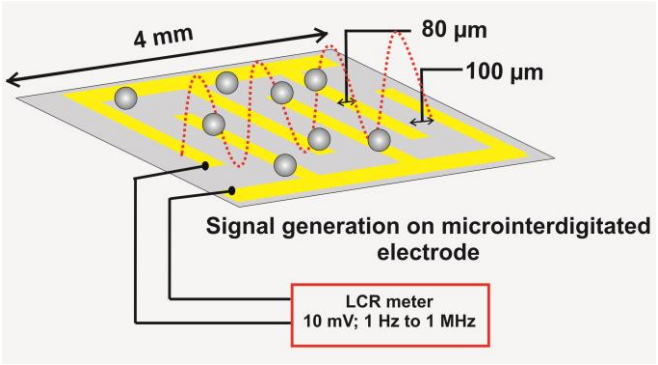

Figure 4. Schematic of the experimental setup used for impedance response measurements of colloidal suspensions. The interdigitated microchip comprised of 80 µm wide finger electrodes with 100 µm edge-to-edge spacing.

Table 1. Effect of medium on the impedance response (ΔZ) of PS colloidal suspensions at 1 MHz for two different particle concentrations. HEPES displayed exceptionally high signal to noise ratio even at low particle fraction.

Medium	**0.01 w/v % PS**	**|S/N|**	**4 w/v % PS**	**|S/N|**
Ultrapure DI water	360.0 ± 212.1	1.70	-2750.0 ± 28.2	97.52
150 mM PBS at pH 7.4	0.2 ± 0.2	1.00	13.4 ± 1.1	12.18
40 mM HEPES at pH 8.5	-10.0 ± 2.5	4.00	58.0 ± 1.5	38.67

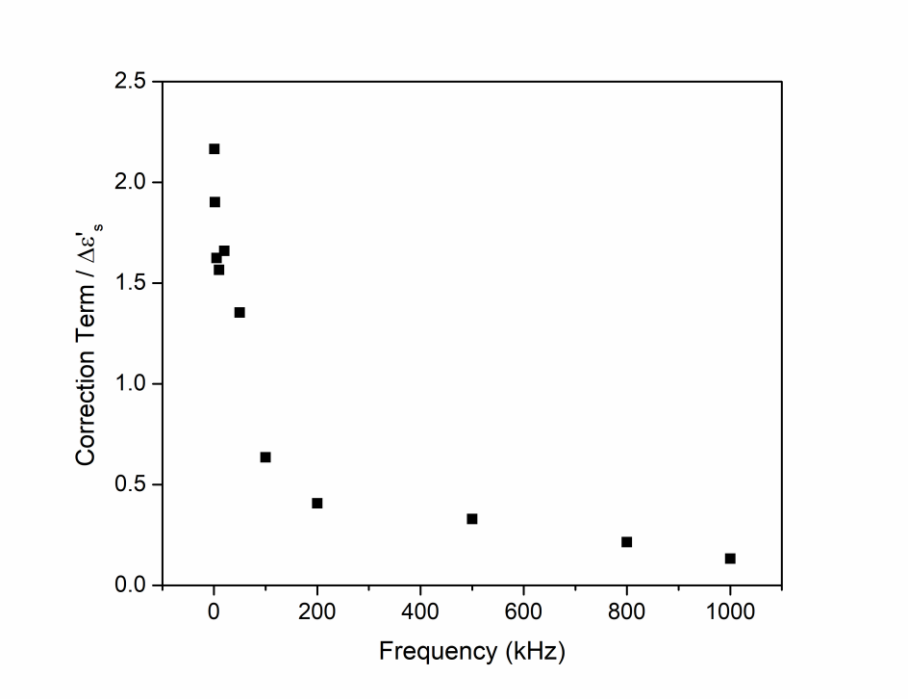

Figure 5. Importance of electrode polarization correction term with respect to the real part of permittivity. Data shown for 2 w/v % Au in HEPES buffer.

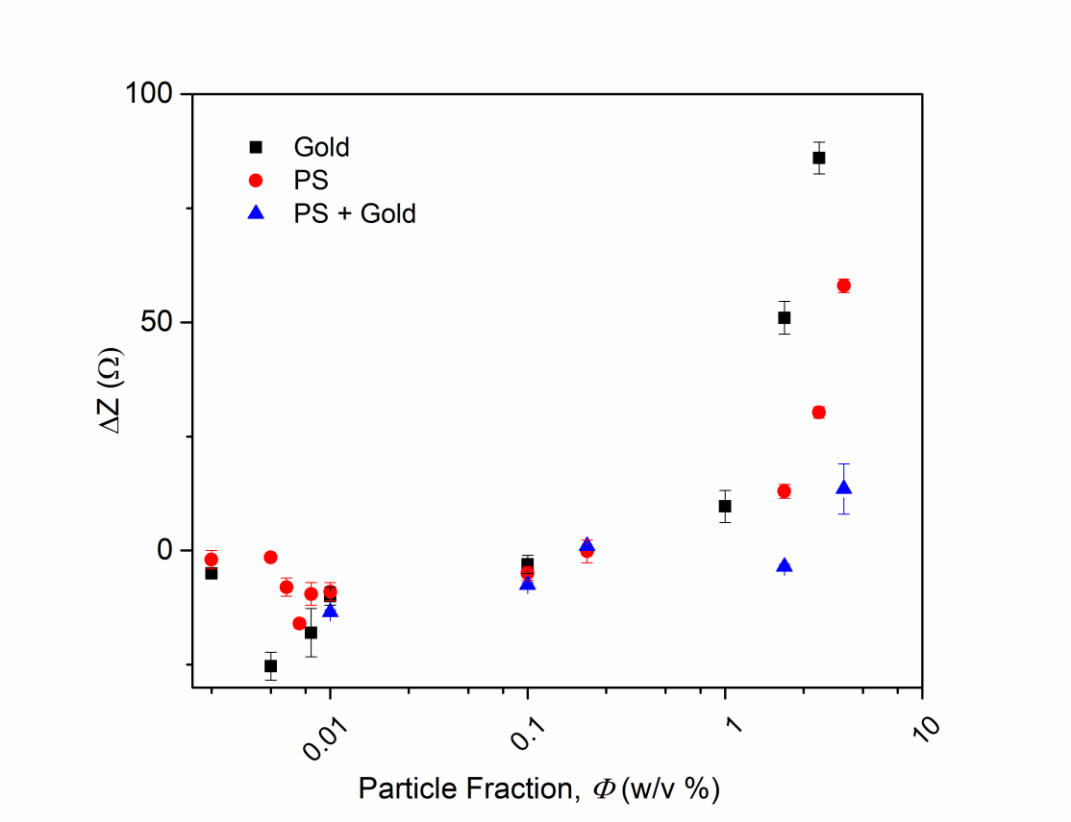

Figure 6. Impedance response of different particle types in HEPES buffer at 1 MHz. The results show generality of non-monotonic behaviour at low concentrations and non-linear signals at high volume fractions.

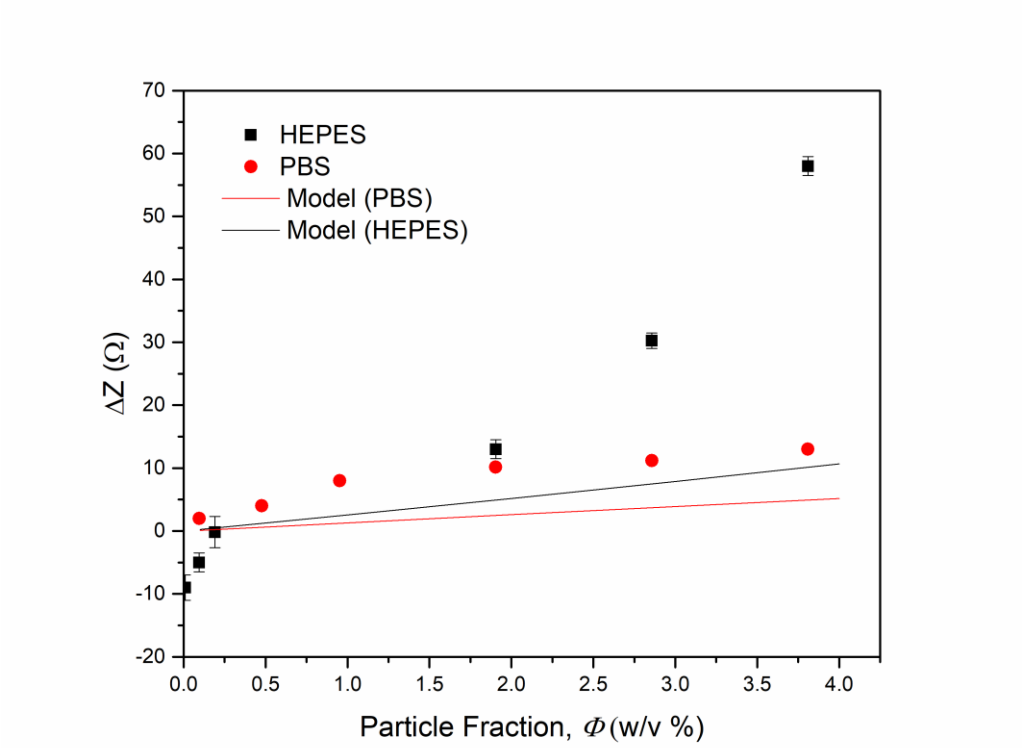

Figure 7. Comparison of analytical model with experimental results obtained in PS suspensions showed good agreement in PBS but no correlation in HEPES.

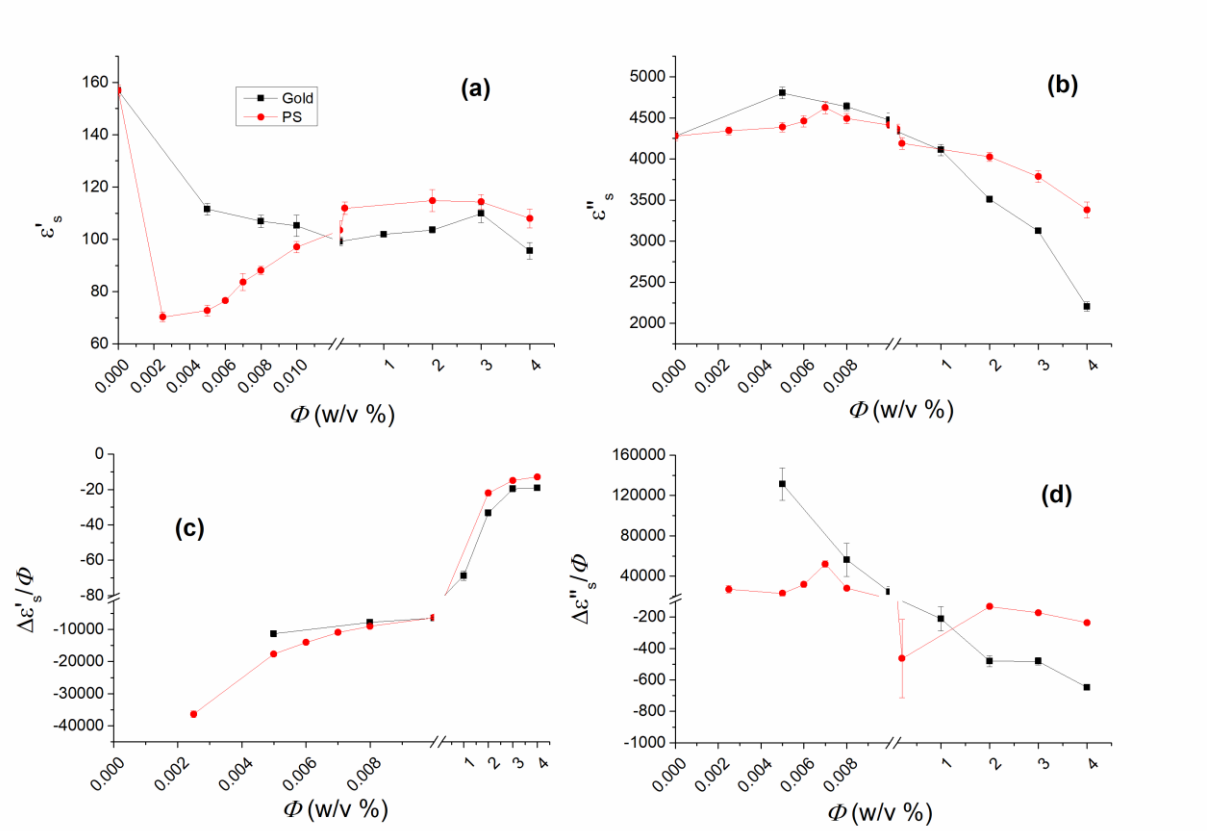

Figure 8. Plot of the real and imaginary parts of the actual and specific permittivities obtained for PS and Au NPs as a function of their concentration at 1 MHz.

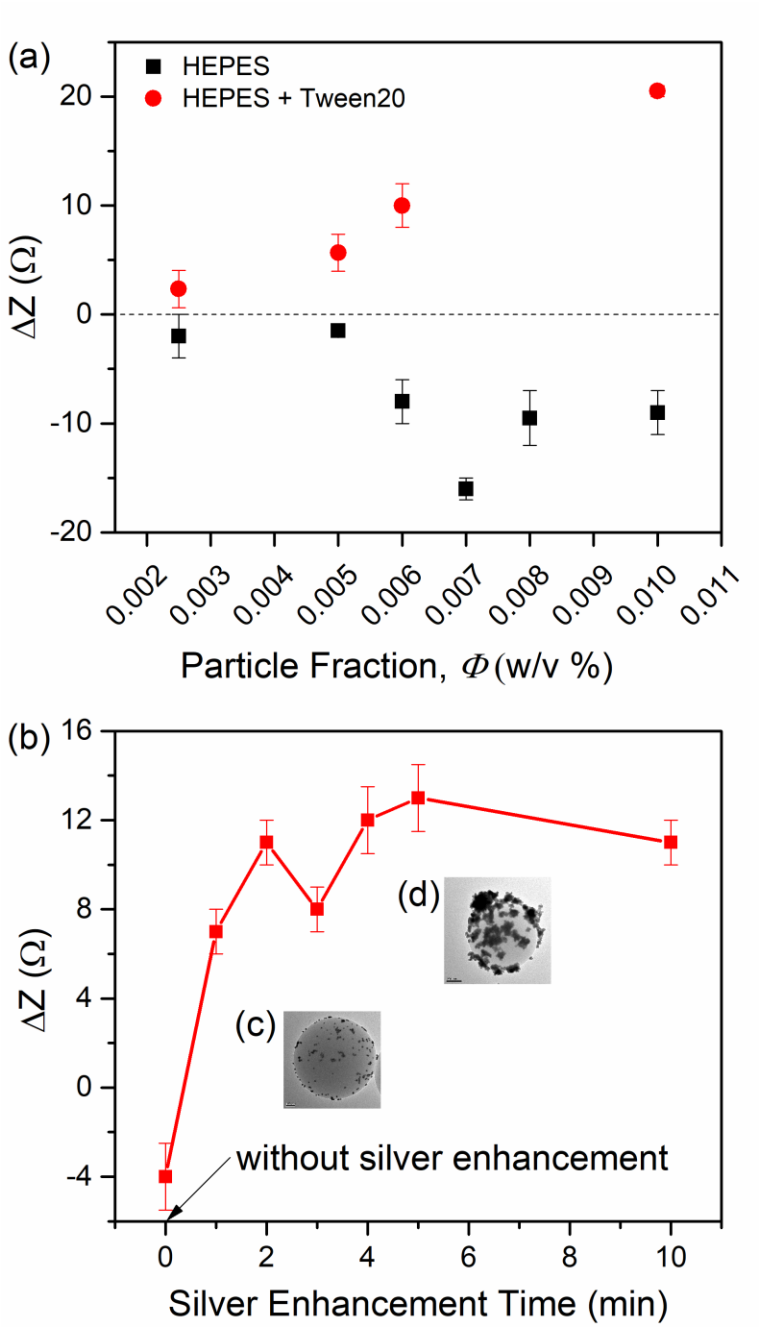

Figure 9. Change in impedance response of PS in HEPES by **(a)** addition of 0.017 % non-ionic surfactant Tween 20 to different particle concentration suspensions and **(b)** deposition of silver metal on Au NPs immobilized over PS particles. The insets show transmission electron microscopy (TEM) images corresponding to **(c)** before and **(d)** after 3 min of silver enhancement.

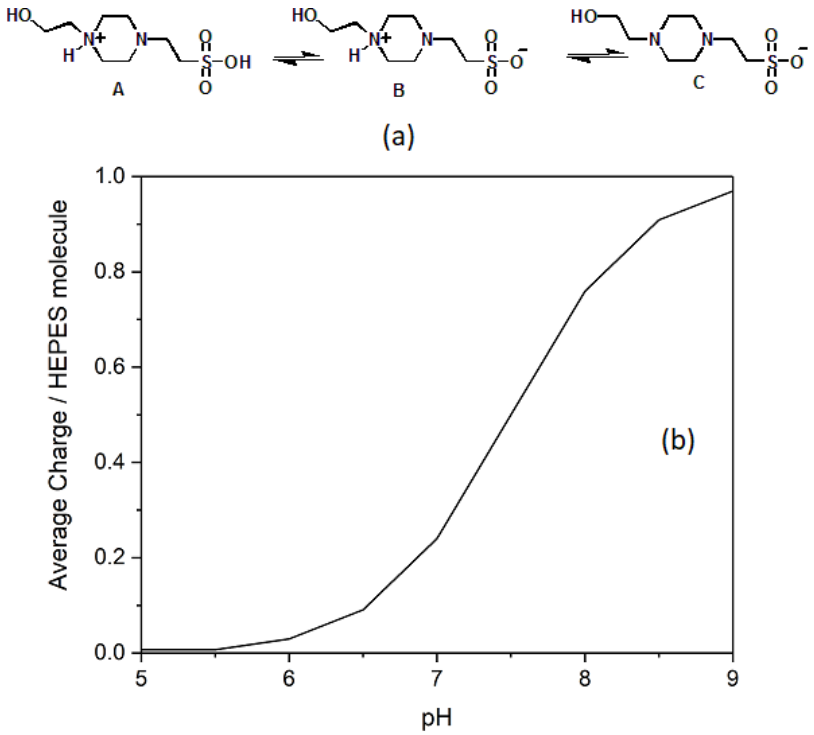

Figure 10. The effect of pH on the zwitterionic form and relative charge on the HEPES molecule. **(a)** Schematic of the molecule in the charged and uncharged states where, A is the predominant state at low pH, B is the intermediate zwitterionic state and C is the major component at higher pH. **(b)** The charge per HEPES molecule as a function of pH. Most of the HEPES molecules exist in the zwitterionic state around pH 5, and the average charge per molecule is close to zero. At pH ≈ 8, we are well above pKa_2 7.5 and hence, we see that most of the HEPES exists in an acidic form with net charge per molecule close to -1.

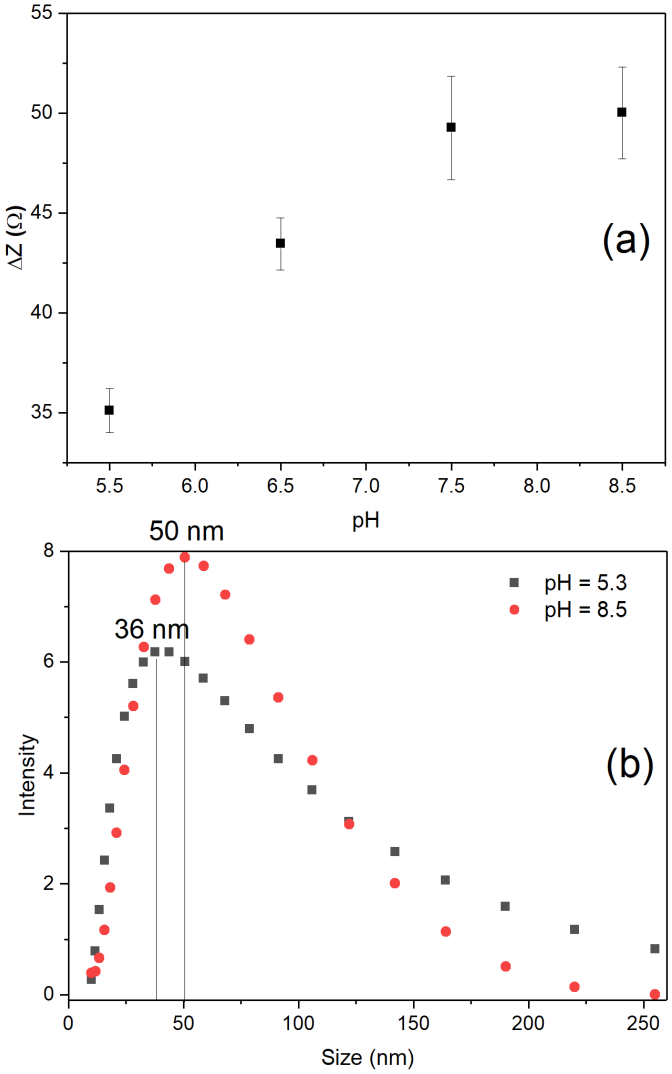

Figure 11. Effect of HEPES buffer pH on the **(a)** impedance and **(b)** hydrodynamic diameter of 2% w/v Au NP suspension. The hydrodynamic size of NPs was measured using DLS.

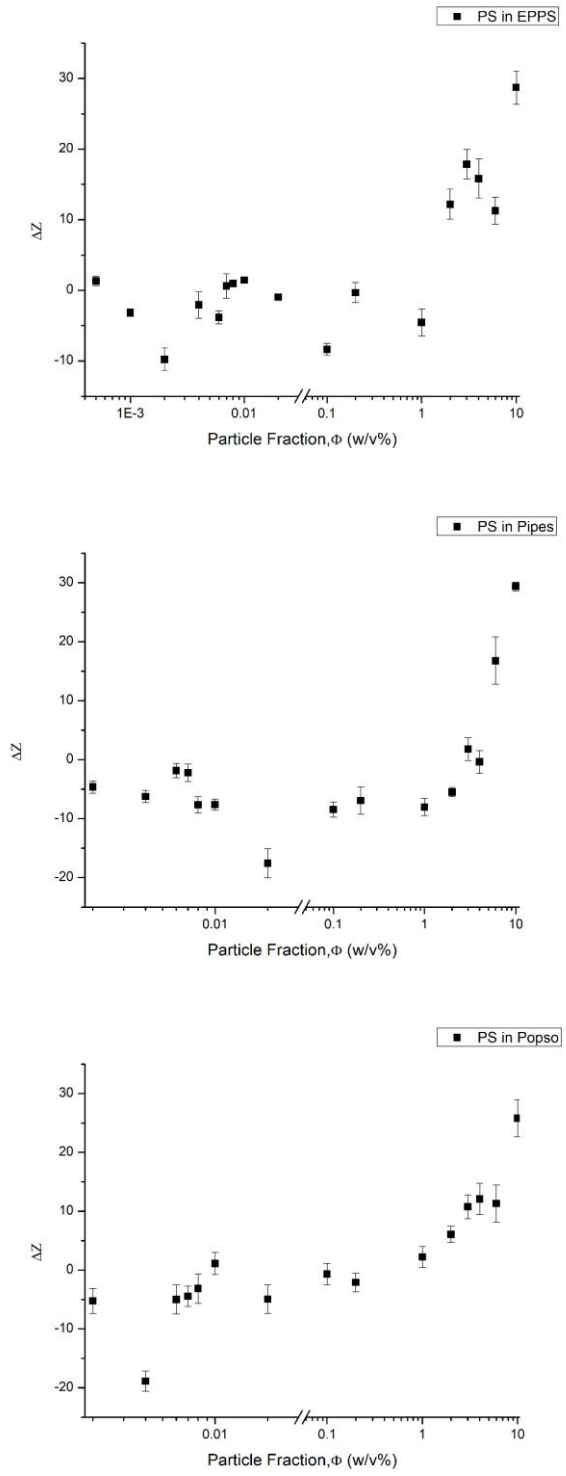

Figure 12. Generality of approach seen with three other zwitterionic buffers: **(top)** EPPS, **(middle)** PIPES and **(bottom)** POPSO.

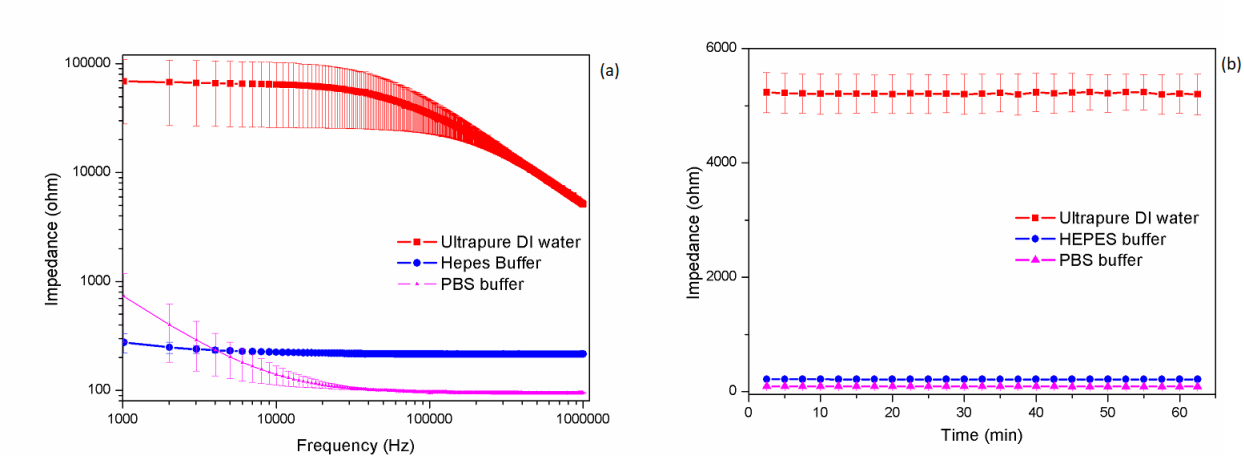

Fig. S1. Impedance spectra as a function of **(a)** frequency and **(b)** time in different media. The results in (a) are reported 5 min after sample loading. Here, the flatness of the HEPES curve unlike water and PBS is suggestive of negligible electrode polarization effects. In (b), the results are reported at f = 1 MHz.

Calculation of working frequency range

Chassagne *et al.* [28] have given expressions for the frequency up to which mobile charges lead to full build-up of double layer at blocking electrodes (ω_P) and the frequency above which the effect of electrode polarization can be completely ignored (ω_b). The two expressions are given as per equations S1 and S2:

$$\omega_P = 2\pi f_P = \frac{2\kappa a D_0}{da} \qquad \textbf{(S1)}$$

$$\omega_b = 2\pi f_b = \sqrt{\omega_0 \omega_P}\,; \omega_0 = D_0\kappa^2 \qquad \textbf{(S2)}$$

where, D_0 is diffusivity of ion, κ^{-1} is Debye length, a is particle radius, and d is electrode gap.

The values of various parameters used to calculate f_P and f_b for a suspension of PS particles in PBS buffer are as below:

Parameter values:	d, m	1.00E-04	a, m	5.00E-07	κa	7.04E+02	$D_0, \frac{m^2}{s}$ 2.00E-09
Electrode polarization frequencies for a suspension of PS particles in PBS buffer					$\omega_P, \frac{1}{s}$	5.63E+04	$\omega_b, \frac{1}{s}$ 1.49E+07
					$f_P, \frac{1}{s}$	8.96E+03	$f_b, \frac{1}{s}$ 2.38E+06

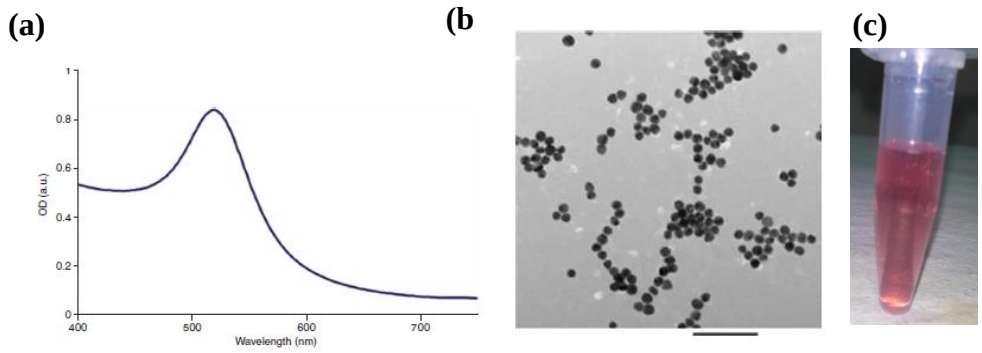

Fig. S2. Characterization of Au NPs: (a) UV-Visible spectrum, **(b)** TEM image and, **(c)** actual digital camera image of an Au NP suspension showing monodisperse particles of size 16 ± 4 nm. The scale bar is 100 nm.

Preparation of metallodielectric particles

The Au NPs were prepared as discussed in the main text and characterized as shown below (**Fig. S2**). Following this, 20 μL of 2% PS suspension was co-incubated with 1 mL of 1.12 nM Au NP suspension. As the time of incubation was increased from 4 h to 24 h, the number of Au NPs attached to the PS beads also increased, or conversely, the number of Au NPs remaining in the supernatant decreased (**Fig. S3a**). To convert the UV-visible spectra into Au NP concentration, we used the following ref*:*[27].

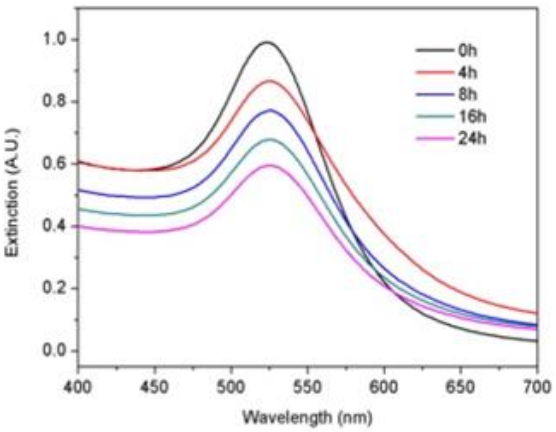

Fig. S3. (a) UV-visible spectra illustrating the concentration of the Au NPs remaining in the supernatant after binding to the PS beads.

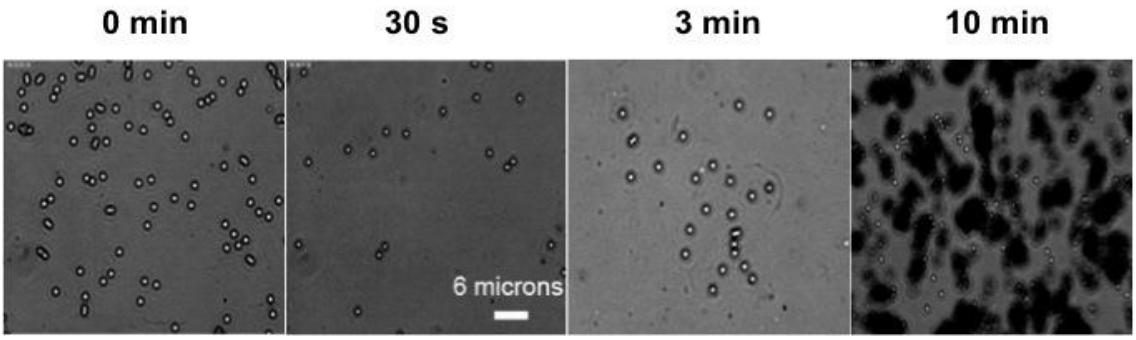

Fig. S4. Time-lapsed optical micrographs of Au-PS particles with increasing durations of silver enhancement. The 2% w/v PS beads were coated with Au NPs via 24 h of incubation process as discussed above. The silver enhancement procedure followed was as per the user manual. All the images were taken using a 100× oil immersion objective mounted on a BX53 optical microscope using a CCD camera (Pixelfly, PCO, Germany). Although the extent of silver coverage on the Au NPs was not quantified, it was observed that the Ag-Au-PS particles had moderate colloidal stability. They precipitated noticeably when stored at 4 ^{o}C beyond a day. The process, however, was reversible as the precipitates could be redispersed via ultrasonication.

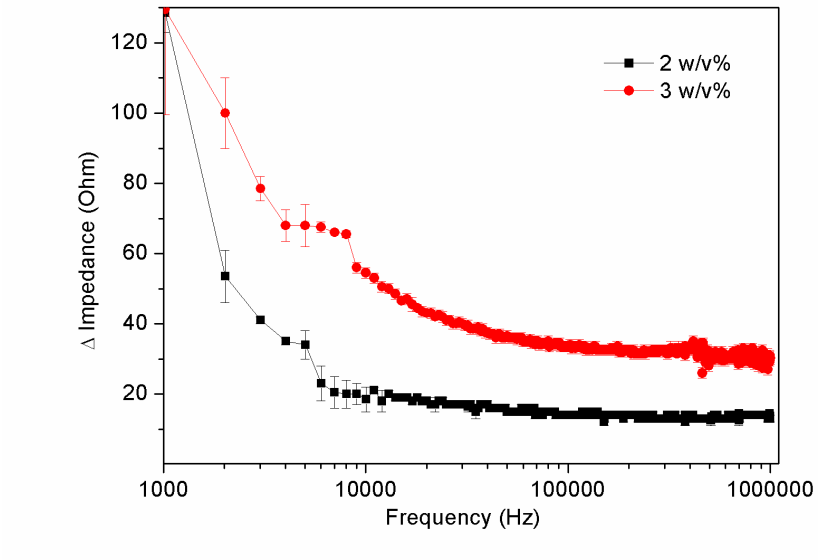

Fig. S5. Experimental values of the dielectric increment as a function of frequency for 2 and 3 w/v % PS particles in HEPES buffer. The graph clearly shows alpha relaxations obtained around 5 and 8 kHz, for 2 and 3 w/v% particles, respectively.

Permittivity and conductivity increment calculations

The complex conductivity ($K^*(\omega)$) of the system was obtained from the experimentally measured impedance values ($Z(\omega)$) using the relation [8] (**eq. 1**)

$$K^*(\omega) = \frac{1}{C_c\, Z_s(\omega)} \qquad (1)$$

where, C_c is the electrode cell constant. It was obtained using the relation, $C_c = KZ$, where, K = 1.29 S/m was obtained by measuring the conductivty of a standard 0.1 M KCl solution at 25 ^{o}C on our chip and Z = 119 Ω was obtained by measuring the impedance of the same KCl solution at 25 ^{o}C on our chip. By doing this, the value of C_c was obtained as 153.5 m^{-1}. The real part of suspension conductivity ($K'_s(\omega)$), which is a measure of resistance in the system, is related to complex conductivity as (**eq. 2**),

$$K_s^*(\omega) = K'_s(\omega) + i\omega\varepsilon_o\varepsilon'_s(\omega) \qquad (2)$$

where, $\varepsilon'_s(\omega)$, the real is part of complex permittivity, is a measure of capacitance in the system. For the buffer alone, this quantity reduces to **eq. 3**,

$$K_e^*(\omega) = K_e + i\omega\varepsilon_o\varepsilon_e \qquad (3)$$

where, K_e is the DC conductivity of the electrolyte and ε_e is the relative dielectric permittivity of the electrolyte solution independent of frequency. The complex permittivity is related to complex conductivity as (**eq. 4**),

$$\varepsilon_S^*(\omega) = \frac{K_S^*(\omega)}{i\omega\varepsilon_o}. \qquad (4)$$

Under the assumption of low concentration or, no particle-particle interactions, the change in complex conductivity or complex permittivity due to a single particle is calculated as per **eq. 5 & 6**, respectively.

$$\frac{\Delta K_S^*}{\emptyset} = \frac{K_S^*(\omega) - K_e^*(\omega)}{\emptyset} \qquad (5)$$

$$\frac{\Delta \varepsilon_S^*}{\emptyset} = \frac{\varepsilon_S^*(\omega) - \varepsilon_e^*(\omega)}{\emptyset} \qquad (6)$$

where, ∅ is the volume fraction of particles in the suspension.

O'Brien's analytical solution

In the limit of thin double layer, O'Brien *et al.* [31] gave the measure of the dipole moment generated by the polarization of the particle core and its double layer as,

$$C_0(\omega) = \frac{(2\lambda - \frac{i\omega\varepsilon_{int}}{K_e}) - (1 - \frac{i\omega\varepsilon_o}{K_e})}{2(1 - \frac{i\omega\varepsilon_0}{K_e}) + (2\lambda - \frac{i\omega\varepsilon_{int}}{K_e})}$$

where, $C_0(\omega)$ is the dipole-coefficient and ε_{int} is the relative permittivity of particle core. The complex permittivity increment $\Delta K_s^*(\omega)$, on ignoring $O(\phi^2)$ and higher terms, is given by,

$$\frac{\Delta K_s^*(\omega)}{\phi} = \frac{3}{a^3}(K_e - i\omega\varepsilon_0)C_0(\omega)$$

To compare this theoretical prediction with experimental data, we subtract a frequency independent offset from only the real part of $\Delta K_s^*(\omega)$, as was done by Beltramo *et al.* [16] The expression for double layer conductivity parameter λ was taken from equation 17 of Mangelsdorf *et al.*[8] when $\exp\left(-\frac{ez_i\xi}{k_bT}\right) \gg 1$ and equation 21 (reproduced below) when this condition is not satisfied. Assuming ions with equivalent mobility (or, diffusivity), the expression for double layer conductivity parameter λ is given by

$$\lambda = \frac{2}{\kappa a}\left(1 + \frac{3m}{z^2}\right)\left[\cosh\left(\frac{ez\xi}{2kBT}\right) - 1\right]$$

$$m = \frac{z_i\,\lambda_{avg}\mu}{e}$$

$$\mu = \frac{\varepsilon_o k_B T}{6\pi\eta_o e}$$

where, λ_{avg} is the average drag coefficient calculated from a composition weighted average of individual drag coefficients, λ_i, given by,

$$\lambda_i = \frac{k_bT}{D_i},$$

where D_i is diffusivity of ion.

Ion	**Ionic diffusivity, m^2/s**
Na^+	1.33×10^{-9}

HEPES ion	5.00×10^{-10}
K^+	1.96×10^{-9}
Cl^-	2.03×10^{-9}
PO_4^{3-}	0.61×10^{-9}

Calculation of Debye lengths (κ^{-1}) in PBS and HEPES buffer

The Debye length was obtained from the relation given by Debye-Huckel theory [33],

$$\kappa^2 = \sum_1^n \frac{e^2 z_j^2 n_j^\infty}{k_b T}$$

where, e represents the charge of an electron, z_j stands for the charge on j[th] ionic species, n_j^∞ is the ionic density for the species far away from the particle, k_b is the Boltzmann constant. n_j^∞ was obtained from the respective concentration of the ionic species.

The concentration of anionic HEPES (A^-) in 40 mM HEPES buffer at pH 8.5 was obtained from the Henderson-Hasselbach equation:

$$pH = pKa + \log\frac{[A^-]}{[HA]}$$

$$8.5 = 7.5 + \log\frac{[A^-]}{[HA]}$$

$[A^-] = 10\,[HA] = 10\left[40 - [A^-]\right] = 36.36$ mM.

The other ionic concentrations are

$[H^+] = 10^{-8.5} = 3.16$ nM

$[OH^-] = 10^{-5.5} = 3.16$ µM

$[Na^+] = 40$ mM

Similar steps were repeated for 150 mM PBS buffer at pH 7.4 which has the composition 137 mM Na^+, 2.7 mM K^+, 139 mM Cl^-, 10 mM PO_4^{3-}. The final vaues obtained are reported in **Table S1**.

Table S1: The values of our system parameters.

Suspension type	Zeta potential (ζ), mV	κa
PS in HEPES	-65	327.74
PS in PBS	-39.5	703.59
Au NP in HEPES	-26.3	5.24

Calculations for amount of Tween 20 added to fully saturate a particle suspension

For a 10 µL 0.1% v/v PS suspension, the total volume of particles in the system,

$$\frac{4}{3}\pi r_p^3 N_p = \frac{0.1\times 10\ \mu l}{100} = 0.01\ \mu l$$

$$\text{Or, } N_p = \frac{0.01}{\frac{4}{3}\pi r_p^3}$$

where, N_p is the total number of particles. So, the total surface area available for surfactant adsorption = $4\ \pi r_p^2 N_p = \frac{0.03\times 10^{-9}}{0.5\times 10^{-6}} = 6 \times 10^{-5}\ m^2$. Now, the cross-sectional area of one Tween 20 molecule ~ 133 A^{o2}.[7] Therefore, the total concentration of Tween 20 required is

$$\left(\frac{6\times 10^{-5}\ m^2}{4\ \pi\ (66.5)^2}\right) \text{ x } \left(\frac{1}{10\times 10^{-6}\ L}\right) = 7.5\ \mu M \text{ or } 0.017\ v/v\%.$$

Since this surfactant amount corresponds to the saturation level in the highest particle concentration suspensions used, we kept this concentration fixed in all our surfactant-based experiments. This meant there would be excess unbound Tween 20 present in solution in all the lower particle concentration cases. To account for the impedance variation due to these remaining molecules, impedance data for all lower concentration suspensions were reported after subtraction of the appropriate baseline, i.e., 7.5 µM – M_{lower}, where, M_{lower} is the saturation concentration for a particular lower concentration (calculated using the same approach as above).

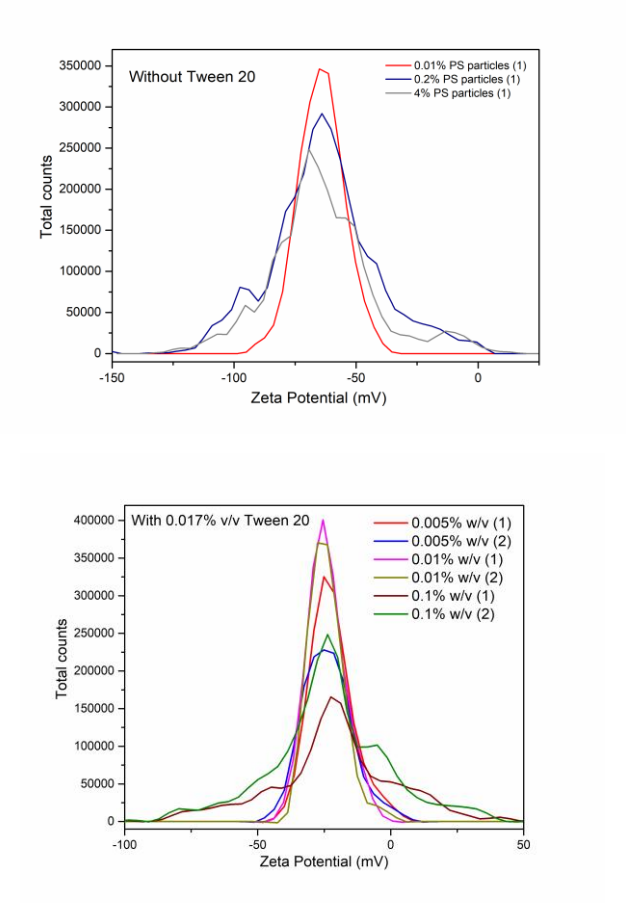

Fig. S6. Zeta potential values of PS particles before and after Tween 20 addition.

(a)

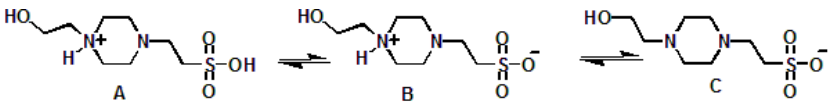

(b)

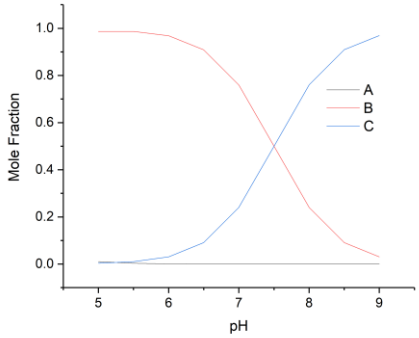

Fig. S7. (a) The different states of HEPES molecule having pKa values at 3 and 7.5, respectively. **(b)** The graph shows the calculated relative mole fraction of each state as a function of pH.

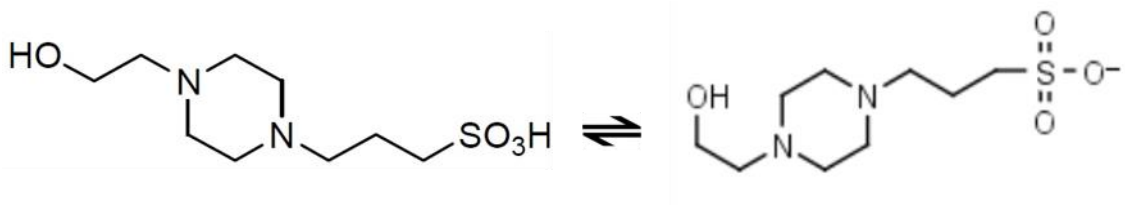

Fig. S8. Molecular structure of EPPS with a single extra carbon atom on the sulfonate side chain as compared to HEPES buffer.